



ELSEVIER

Nuclear Physics A 694 (2001) 559–589



www.elsevier.com/locate/npe

Positron polarization in the decay of polarized ^{12}N : a precision test of the Standard Model

E. Thomas^{a,*}, R. Prieels^a, M. Allet^{b,1}, K. Bodek^{b,2}, J. Camps^{d,3},
J. Deutsch^a, F. Gimeno-Nogues^{a,4}, J. Govaerts^a, J. Lang^b,
O. Naviliat-Cuncic^{b,5}, I. Pepe^{a,6}, P. Quin^c, N. Severijns^d, J. Sromicki^{b,7}

^a *Université catholique de Louvain, B-1348 Louvain-la-Neuve, Belgium*

^b *Eidgenössische Technische Hochschule, Zürich, Switzerland*

^c *University of Wisconsin, Madison, USA*

^d *Katholieke Universiteit Leuven, Leuven, Belgium*

Received 12 February 2001; revised 5 April 2001; accepted 17 April 2001

Abstract

The longitudinal polarization of positrons emitted along and opposite to the nuclear spin direction has been measured in the decay of polarized ^{12}N . The results are consistent with the Standard Model prediction. In manifest left–right symmetric models this measurement provides a lower bound of $310 \text{ GeV}/c^2$ at 90% CL on the mass of a possible right-handed gauge boson contributing to the electroweak interaction. In generalized versions of this model our measurement provides constraints complementary to those set by high-energy experiments. © 2001 Elsevier Science B.V. All rights reserved.

PACS: 13.10.+q; 23.40.Bw; 24.70.+s; 27.20.+n

Keywords: Standard Model; Longitudinal polarization; W_R constraints; polarized ^{12}N ; Positronium time-resolved spectroscopy

* Corresponding author. Presently at INFN, Laboratori Nazionali di Frascati, Italy.

E-mail address: eric.thomas@lnf.infn.it (E. Thomas).

¹ Presently at AluSuisse, Sierre, Switzerland.

² On leave from Jagellonian University, Cracow, Poland.

³ Presently at St Elisabethziekenhuis, Turnhout, Belgium.

⁴ Presently at Benelux Assist sa., Brussels, Belgium.

⁵ Presently at LPC Caen, France.

⁶ Collège de France, Paris, France; on leave from Univ. Federal de Bahia, Brazil.

⁷ Presently at Kantonsschule Sursee, Switzerland.

1. Introduction

The $SU(2)_L \times U(1)_Y$ Standard Model of the electroweak interaction is spectacularly successful [1]. However, given some of its ad-hoc assumptions and the number of free parameters, it is considered to be only a low-energy approximation of a more general theory, and efforts are undertaken to find deviations from it, which would lead the way to more global unification schemes [2]. Most of such tests are performed at high energies, but the interest and complementarity of precision experiments at low energies ought also to be stressed [3].

Here, such a low-energy precision experiment is described: the measurement of the longitudinal positron polarization in the decay of polarized ^{12}N nuclei. This is an improved follow-up of an earlier experiment performed by our collaboration [4]. It is similar, in its principle, also to the one performed on ^{107}In [5]. This section emphasizes the specificity of this experiment compared to other beta-decay symmetry tests, while in section 6 all such results shall be combined and discussed appropriately.

The observable considered here was first suggested by P. Quin and T. Girard [6] and consists in comparing the longitudinal polarizations of the decay electrons (positrons) emitted parallel, P^+ , and antiparallel, P^- , to the spin of the emitting nucleus.

Being a relative measurement, this experiment thus avoids to first order having to determine the analyzing power of the polarimeter. Furthermore, it is very sensitive to physics beyond the Standard Model [7,8] especially for pure Gamow–Teller transitions, as is the case with ^{12}N . Ignoring recoil order contributions, the Standard Model value of the polarization ratio R_0 for two opposite polarizations of the emitting nucleus takes the form

$$R_0 = \left(\frac{P^-}{P^+} \right)_0 = \frac{1}{1 - A_{\text{exp}}} \left[\frac{\beta^2(2 - A_{\text{exp}}) - A_{\text{exp}}}{\beta^2(2 - A_{\text{exp}}) + A_{\text{exp}}} \right], \quad (1)$$

where β is the positron velocity and A_{exp} the experimental asymmetry defined by

$$A_{\text{exp}} \stackrel{\text{def}}{=} 1 - \frac{r_{\beta}^-}{r_{\beta}^+}, \quad (2)$$

r_{β}^- (respectively r_{β}^+) being the count rates of positrons incident on the polarimeter when the nuclear polarization is opposite (respectively parallel) to their direction of emission. The ratio of the experimental value $R \stackrel{\text{def}}{=} P^-/P^+$ compared to the Standard Model prediction R_0 is then

$$\frac{R}{R_0} = 1 - k \frac{\Delta}{1 + 4 \frac{A_{\text{exp}}}{\beta^2(2 - A_{\text{exp}}) + A_{\text{exp}}} \Delta} \simeq 1 - k \Delta, \quad (3)$$

where Δ is a measure of a deviation from the Standard Model and

$$k = 8 \frac{\beta^2(2 - A_{\text{exp}})}{\beta^4(2 - A_{\text{exp}})^2 - A_{\text{exp}}^2} \quad (4)$$

an enhancement factor which can be large if A_{exp} is close to unity (i.e. if the transition is well chosen and the polarization sizeable). An enhancement factor of $k = 5\text{--}7$ was readily achieved in the study of ^{107}In [5].

In the experiment reported here the enhancement factor was smaller because of the lower nuclear polarization achieved (Section 2.3.1), but this was compensated by better statistics leading to an improved result compared to the previous ones. Moreover the evaluation of recoil corrections is based on experimental inputs (Section 2.3.2), while the possible systematic errors are different and well under control (Section 5).

The experiment is described in Section 2, the data analysis in Section 3, and Sections 4 and 5 address the limits obtained for the parameter Δ . Finally Section 6 shows how our result constrains various scenarios beyond the Standard Model, with Section 7 presenting our main conclusions.

2. The experiment

As can be seen from (3), the experiment measures the ratio R of the polarization of positrons emitted parallel and antiparallel to the spin of the decaying nucleus, and compare this value of R to that, R_0 , which is expected within the Standard Model. The evaluation of R_0 in (1) requires the measurement of the positron velocity β and of the emission asymmetry A_{exp} , see (2). These quantities enter also the expression of the enhancement factor k , see (4) which sets the scale of sensitivity of the experiment to deviations from the Standard Model through $\Delta \neq 0$. In the following, the experimental set-up and the procedure used to optimize and measure these quantities are described.

2.1. The experimental set-up

The experimental set-up can be divided into three main components: a target where the polarized ^{12}N nuclei are produced; a spectrometer for momentum selection of the emitted positrons; and a polarimeter where the positron polarization is analyzed. Fig. 1 presents a schematic view of the experimental set-up. Polarized ^{12}N nuclei were produced through the $^{12}\text{C}(\vec{p}, n)^{12}\vec{\text{N}}$ polarization transfer reaction. This reaction was initiated using a 21.4 MeV, 76% transversely polarized proton beam from the Injector-I cyclotron of the Paul Scherrer Institute (Villigen, Switzerland) which is equipped with an atomic-beam-type polarized ion source. The polarization of the beam could be reversed rapidly by stimulating two different radio frequency transitions in the ion source.

The target consisted of a stack of 80 carbon and 80 aluminum foils of thickness $100 \mu\text{g}/\text{cm}^2$ and $400 \mu\text{g}/\text{cm}^2$, respectively, placed in a 3.8 kG magnetic field B_H to hold the nuclear polarization (see Fig. 1). The stack-arrangement allowed the bulk of the ^{12}N reaction products to recoil and to stop in the aluminum catchers where their residual polarization was larger than in carbon (see Fig. 2 and Ref. [9]). The polarization ratio R_0 (1) and enhancement factor k (4) depend on the effective mean asymmetry measured experimentally. This asymmetry is function of the relative amount of recoiling ^{12}N ions stopping in carbon or in aluminum but to extract our result this amount does not have to be known.

The beam energy was chosen to optimize the polarization transfer (see Fig. 2 and Ref. [9]), to optimize the ^{12}N production rate [10] and to be below the 26.2 MeV threshold

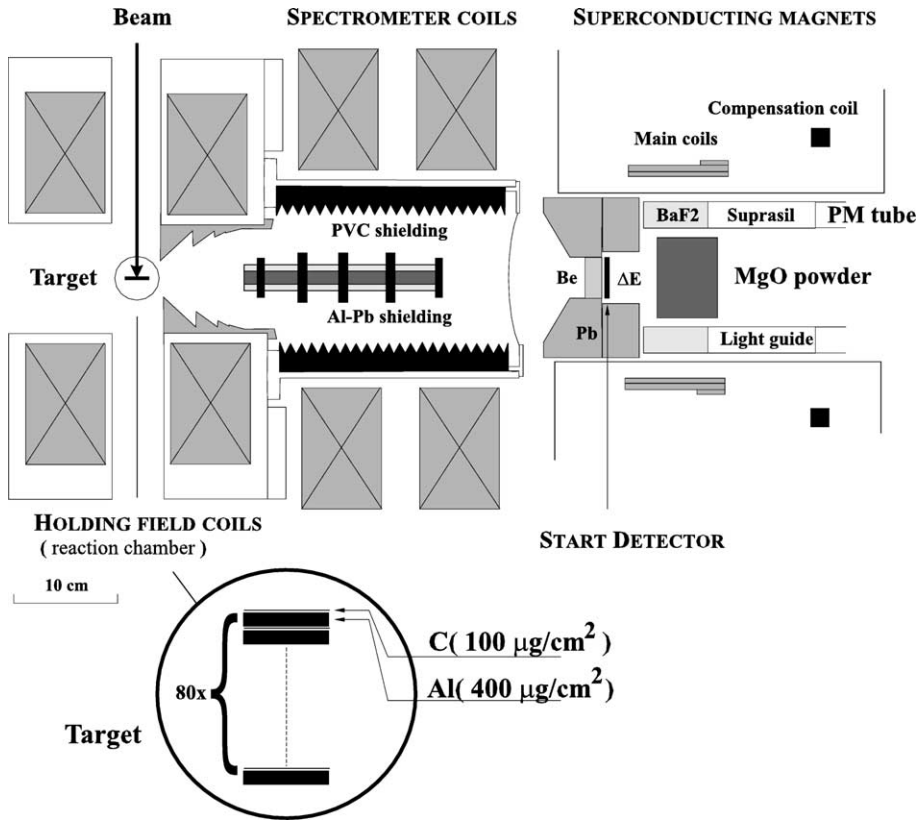


Fig. 1. Schematic view of the experimental set-up.

of the $^{12}\text{C}(p, \alpha n)^8\text{B}$ contaminant reaction [11]. Indeed, if present the β^+ arising from the ^8B decay ($E_0 = 14.1$ MeV) could not be separated in momentum from the decay of ^{12}N ($E_0 = 16.3$ MeV). The purity of the ^{12}N source was checked by measuring the decay rate during eleven ^{12}N half-lives (see Fig. 3).

The shape and the materials of the inner walls of the spectrometer were chosen to reduce scattering of positrons. The mean energy of the selected positrons is 6.0 MeV with a momentum resolution of 17%. The angular acceptance ranges from 7 to 23 degrees.

The polarization of positrons is measured using time-resolved spectroscopy of positronium annihilation in a strong magnetic field. For a detailed description of the method we refer to Refs. [12–17] and recall here only those features which are essential to understand what follows.

Positrons signal their arrival into a fine-grained MgO powder⁸ compressed to a density of 0.58 g/cm^3 , by passing through a 0.5 mm thick plastic scintillator, the “start-detector” in Fig. 1. Some 42% of these positrons form positronium in the MgO powder. Since the powder is placed in a strong magnetic field (9.3 kG), the two $m = 0$ hyperfine sublevels

⁸ The MgO powder had a mean grain size of 100 \AA , E. Merck, Darmstadt, DE, Ref. 5862.

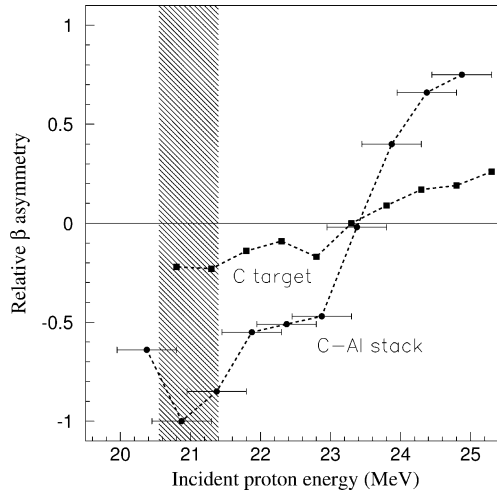


Fig. 2. Relative β asymmetry as a function of the incident proton beam energy, normalized to its largest absolute value. Circle data points correspond to the β asymmetry measured using the C–Al stack target; square data points give the β asymmetry for a pure C target. Horizontal error bars indicate the energy dispersion of the protons in the target. The shaded region corresponds to the energy range of the present measurement. For the corresponding value of the β asymmetry see the value of A_{exp} in the Section 2.3.1. The dotted lines are drawn to guide the eye and do not represent experimental data; sharp resonances between the available data points cannot be excluded.

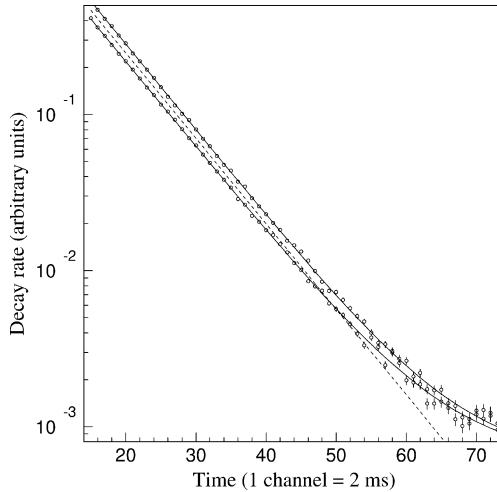


Fig. 3. $\beta\gamma$ count rate in arbitrary units for opposite polarization directions as a function of time over a period extending up to eleven ^{12}N half-lives. The straight line represents the world average ^{12}N half-life [11]. After a long period, one observes the presence of a low intensity unpolarized background of long lifetime. Its relative amplitude at time $t = 0$ is $(9.93 \pm 0.32) \times 10^{-4}$. Assuming that the relative amplitude of this background scales with the average beam intensity, it represents $(3.92 \pm 0.11) \times 10^{-3}$ of the count rate during window-A and $(11.12 \pm 0.34) \times 10^{-3}$ during window-B (see Section 2.2). The systematic effect arising from this unpolarized background is estimated in Section 5.

get mixed to form a short lived “pseudo-singlet” and a longer lived “pseudo-triplet” state. In our conditions the amplitude of this pseudo-triplet component of interest is proportional to $(1 - 0.25 \vec{P} \cdot \hat{B})$ where \vec{P} is the positron polarization along the magnetic axis and \hat{B} the magnetic field direction at the positronium formation location. Its lifetime is about 7.5 ns and can easily be separated both from the prompt annihilation peak mixed in the pseudo-singlet component and from the decay of the unperturbed ($F = 1$, $m = \pm 1$) levels which have in vacuum a lifetime of 142 ns but are quenched in the MgO powder to about 123 ns. The pseudo-triplet state undergoes a mixed decay by emitting 2 photons 95% of the time and 3 photons 5% of the time.

About 1% of the positrons which trigger the scintillator, stop in the plastic scintillator and are accounted for in the analysis.

The stopping medium is surrounded by six hexagonal (\varnothing 37 mm \times 60 mm) BaF₂ scintillators which signal the arrival of an annihilation photon. The experiment consists in the observation of the annihilation time-spectrum $N_{\beta\gamma}(t)$ and of its modification upon rapid inversions of the ¹²N polarization.

The time response function of the start-stop system and associated electronics, and the amount of positrons stopping in the plastic, are measured by replacing the MgO powder by pure aluminum of the same macroscopic density in which no positronium formation takes place and thus provides a source of practically “prompt” positron annihilations only.⁹

2.2. Experimental procedure

The experiment implements a succession of many identical cycles. One cycle consists of the following sequence: the target is irradiated during 25 ms followed by a 3 ms waiting period. Following that, data are then accumulated during 36 ms. After 20 such irradiation-measurement cycles, the beam polarization and consequently the ¹²N polarization is reverted, in order to measure with the same device the positron polarization corresponding to two opposite nuclear polarizations.

For the forthcoming discussion it should be emphasized that the observation period after irradiation was split into two time windows: a “window-A” from 4 to 12 ms and a “window-B” from 13 to 40 ms. The aim of this procedure was to perform two practically independent experiments with two different source strengths providing for an overall cross check on possible intensity related systematic effects.

The positron-start to photon-stop time interval distributions are built in four sectors of an histogramming memory depending on the A and B window and on the parallel or antiparallel polarization of the ¹²N nucleus. Every 20 cycles the content of the histogram memory is dumped onto tape. These spectra are then added within files corresponding to about 2 hours of data taking. Typical acquisition rates are given in Table 1.

In principle, it is possible to measure the polarization ratio P^-/P^+ for opposite ¹²N polarizations with a single orientation of the polarimeter magnetic field only. Using a crude estimate of the analyzing power ($\epsilon = 0.25$), it is possible to extract the polarization ratio

⁹ An annihilation lifetime of 250 ps in Al was assumed in good agreement with the indications of Ref. [18].

Table 1

Typical rates: in the start-detector (β), in the sum of the six BaF₂ scintillators (γ), and in the coincidence of both in a time window of 400 ns (β - γ)

	Window-A	Window-B
β	$5.8 \times 10^4 \text{ s}^{-1}$	$2.7 \times 10^4 \text{ s}^{-1}$
γ	$1.6 \times 10^5 \text{ s}^{-1}$	$1.2 \times 10^5 \text{ s}^{-1}$
β - γ	$1.4 \times 10^4 \text{ s}^{-1}$	$0.6 \times 10^4 \text{ s}^{-1}$

P^-/P^+ from the ratio of the pseudo-triplet populations measured with a single polarimeter magnetic field orientation:

$$\frac{1 + \epsilon P^-}{1 + \epsilon P^+} \approx 1 - \epsilon P^+ \left(1 - \frac{P^-}{P^+}\right) \quad \text{or} \quad (5)$$

$$\frac{1 - \epsilon P^-}{1 - \epsilon P^+} \approx 1 + \epsilon P^+ \left(1 - \frac{P^-}{P^+}\right). \quad (6)$$

However, inverting the field of the polarimeter has two advantages: it allows to estimate the analyzing power using the asymmetry of the pseudo-triplet population and it exactly inverts the sign of the measured effect. Combining (5) and (6), it is then possible to extract the ratio P^-/P^+ free of all possible systematic errors correlated to the nuclear spin reversal, provided, of course, that these are identical for both field configurations:

$$S \stackrel{\text{def}}{=} \frac{1 + \epsilon P^-}{1 + \epsilon P^+} \bigg/ \frac{1 - \epsilon P^-}{1 - \epsilon P^+} \approx 1 - 2\epsilon P^+ \left(1 - \frac{P^-}{P^+}\right). \quad (7)$$

The polarization ratio P^-/P^+ can be obtained from this superratio S of the pseudo-triplet populations and from the knowledge of the analyzing power ϵP^+ : inverting (7) gives

$$\frac{P^-}{P^+} = 1 + \frac{1}{2\epsilon P^+} (S - 1). \quad (8)$$

Therefore, during the run, the magnetic field of the polarimeter was inverted twice, in order to accumulate the same statistics for each polarimeter field orientation.

2.3. Normalization

2.3.1. Extraction of the parameter R_0

One of the strongest points of the present polarization-asymmetry correlation measurement is that its sensitivity to the deviation Δ from the Standard Model may be expressed [6] as a function of the positron asymmetry and velocity (1)–(4). The positron asymmetry A_{exp} is a direct observable of the measurement while, given the momentum selection of our spectrometer–polarimeter set-up, we have $\beta \approx 1$.

Since the polarimetry is based on positronium annihilation, we identified the quantities r_{β}^- and r_{β}^+ entering (2), with the count rates $N_{\beta\gamma}^-(t)$ and $N_{\beta\gamma}^+(t)$ integrated in the observation window of 400 ns.

The experimental asymmetry was $A_{\text{exp}} = 0.2352 \pm 0.0001$ (respectively 0.2264 ± 0.0001) on average during the A (respectively B) measurement windows. The 4% relative decrease in the asymmetry between the A and B windows is due to the relaxation of the ^{12}N polarization ($\tau_{\text{relax}} = 412 \pm 108$ ms) and to the larger fraction of long lived unpolarized background in the B window (see Fig. 3). A_{exp} was computed from coincidence rates measured by scalers and corrected for the dead time of the data acquisition system. The dead time correction increased the value of A_{exp} by 0.01 and 0.005 in A and B window, respectively. False asymmetry, induced by a change of the beam intensity correlated with beam polarization reversal, was controlled by monitoring the beam current during the measurement. Possible false asymmetry from beam intensity was found to be lower than 2×10^{-4} , corresponding to a possible error on R_0 (11) of 2×10^{-6} . The average velocity of the selected positrons is $\beta = 0.9964 \pm 0.0001$, a value which was determined through a Monte Carlo simulation of the trajectories through the apparatus. Using these values, (1) and (4) give

$$\begin{aligned} R_0 &= 0.99804 \pm 0.00006 \quad \text{and} \quad k = 1.0936 \pm 0.0006 \quad (\text{window-A}), \\ R_0 &= 0.99812 \pm 0.00006 \quad \text{and} \quad k = 1.0459 \pm 0.0006 \quad (\text{window-B}). \end{aligned} \quad (9)$$

One may notice that if right-handed currents are contributing in such a way that $\Delta \neq 0$, R_0 is in fact no longer the longitudinal polarization ratio predicted by the Standard Model, since right-handed currents contribute to the experimental asymmetry [19]. Nonetheless, (1)–(4) remain valid.

2.3.2. Systematic corrections to R_0 and k

Eqs. (1)–(4) refer to the average value of the positron spin along its momentum, for a large ensemble of positrons all emitted with the same momentum \vec{p} . In practice however, one has to take into account some experimental contingencies. The spectrometer–polarimeter system has a finite momentum acceptance and, in addition, it is not the longitudinal polarization at emission which is measured by the experimental device represented in Fig. 1, but rather the spin component along the local polarimeter axis (i.e. the magnetic field direction at the location where the positronium state is formed and decays). Due to scattering and magnetic field inhomogeneities, the spin component along the z symmetry axis of the polarimeter is not constant between the positions of positron emission and polarization measurement in the polarimeter. If \mathcal{R} is the spin rotation matrix and $\epsilon(\vec{r})$ the local analyzing power of the polarimeter, the measured polarization can be expressed as [20]

$$\begin{aligned} P(\vec{J}) &= \frac{1}{\langle 1 \rangle + A\langle \beta(\hat{p} \cdot \vec{J}) \rangle + \langle \frac{m}{E} b \rangle} \\ &\quad \times \langle \epsilon(\vec{r}) \hat{n} \cdot \mathcal{R}[\beta G \hat{p} + N \vec{J} + Q^*(\hat{p} \cdot \vec{J}) \hat{p} + \beta R(\hat{p} \times \vec{J})] \rangle, \end{aligned} \quad (10)$$

where \vec{J} is the nuclear polarization vector of the emitting nucleus, $\langle \rangle$ stands for the average over the initial position and momentum distributions of the positrons selected by the spectrometer–polarimeter set-up, $\epsilon(\vec{r})$ is the local analyzing power at the positron stop position, and \hat{n} is a unit vector parallel to the local magnetic field. Finally, A , b , G , N , Q^*

and R are defined in the usual way in terms of the basic four-Fermi nucleonic effective coupling coefficients [6,19,21].

The spin rotation in the spectrometer-polarimeter system was calculated by a Monte Carlo simulation, whose details are discussed in Appendix A. Taking into account these spin rotation and acceptance effects, the values for R_0 and k are modified such that finally

$$\begin{aligned} R_0 &= 0.99672 \pm 0.00024 \quad \text{and} \quad k = 1.0991 \pm 0.0012 \quad \text{for window-A,} \\ R_0 &= 0.99686 \pm 0.00022 \quad \text{and} \quad k = 1.0511 \pm 0.0012 \quad \text{for window-B.} \end{aligned} \quad (11)$$

It is important to note that these corrected values (11) are only slightly different from the uncorrected ones (9). The correction to R_0 is about three times smaller than the statistical error on R (22). The following systematic errors on the evaluation of R_0 have also been considered: (1) the beam displacement on the target, and, (2) the omission of bremsstrahlung in the Monte Carlo evaluation of the spin rotation of positrons traveling through matter. In absolute terms, the first effect was found to be smaller than 1×10^{-4} , while the second should be much less than the full influence of spin rotation in stopping media which amounts to only 8×10^{-4} .

Recoil order terms are well measured in the $A = 12$ triad [22]. Using the expressions given in Ref. [23], their main impact is a slight correction to R_0 . This correction amounts to 0.000138 ± 0.000004 in window-A and to 0.000132 ± 0.000004 in window-B and was already included as well into the final values in (23).

3. Data analysis

Before detailing the analysis procedure, it should be stressed that all data were first corrected for their accidental content. The subtraction procedure and its consequences for the final result are addressed in Section 5.5. Hence, the relations and discussion hereafter apply to spectra from which accidental events have already been subtracted.

3.1. Time response function

The time response function was measured by replacing for one hour every eight hours the MgO powder by an aluminum dump. In order to extract the response function from these aluminum data, one has to account for the fact that the real time distribution of the measured events is not a $\delta(t)$ function, but rather a sum of two exponential functions stemming from the short lifetime of free positrons in aluminum and of positronium formed in the plastic start-detector. The time spectrum taken with the aluminum dump N_{Al} is described by the convolution (denoted by the symbol \otimes) of the positronium decay curve with the response function

$$N_{Al}(t) = F(t) \otimes \left[\frac{n_{Al}}{\tau_{Al}} e^{-t/\tau_{Al}} + \frac{n_{Pl}}{\tau_{Pl}} e^{-t/\tau_{Pl}} \right], \quad (12)$$

where τ_{Al} is the positron lifetime in aluminum, τ_{Pl} the lifetime of positronium formed in the plastic detector, n_{Al} and n_{Pl} the integrals of these two exponential components.

The time response function $F(t)$ is extracted through a fit to $N_{Al}(t)$. The values for τ_{Al} and τ_{Pl} were set to 0.250 ns and 2.0 ns, respectively, according to those found in the literature [18]. The relative amount of the positrons stopped in the plastic counter was fixed by independent measurements (see Section 3.2). The free parameters are the ones describing the response function. Four independent gaussian functions (free, mean and width) and a long exponential tail due to after pulses (free, amplitude and time constant) were needed to describe the response function.

3.2. Determination of the relative amount of positrons stopping in plastic

The relative amount of positrons stopping in the 0.5 mm thick plastic scintillator was determined by inserting plastic disks downstream of the start-detector. Four aluminum spectra $N^i(t)$ were thus recorded with $i = 0.5, 2.5, 4.5, 6.5$ mm of additional plastic. Those measurements were normalized to unity and simultaneously fitted to

$$N^i(t) = F(t) \otimes \left(\frac{(1 - c^i n_{Pl}^{0.5mm})}{\tau_{Al}} e^{-t/\tau_{Al}} + \frac{c^i n_{Pl}^{0.5mm}}{\tau_{Pl}} e^{-t/\tau_{Pl}} \right), \quad (13)$$

where n_{Pl}^i is the relative amplitude of the plastic component and $c^i = n_{Pl}^i/n_{Pl}^{0.5mm}$. The simultaneous fit of those four spectra is shown in Fig. 4. The values for τ_{Al} and τ_{Pl} were set to 0.250 ns and 2.0 ns, respectively, while the c^i coefficients were obtained from Monte Carlo calculations based on the GEANT code [24]. The free parameters of the fit are the response function $F(t)$ and $n_{Pl}^{0.5mm}$. The result of the fit gives $n_{Pl}^{0.5mm} = (6.01 \pm 0.02) \times 10^{-3}$ and is independent of the number of gaussian functions used to describe the response function.

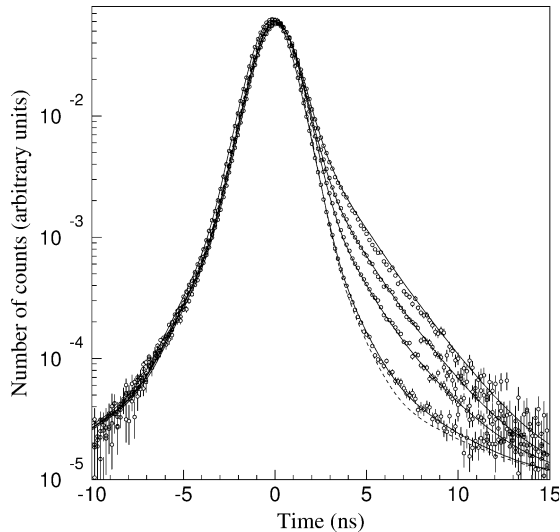


Fig. 4. Simultaneous fit of the time spectra recorded with the aluminum dump and four different thicknesses of plastic disks at the start-detector location. The dashed line is the response function $F(t)$. Count rates are in arbitrary units.

3.3. Pseudo-triplet amplitudes

As explained in Section 2.1, the amplitude of the pseudo-triplet component in the positronium decay spectrum is directly related to the positron polarization, so that its determination is at the heart of the experiment. This pseudo-triplet component is obtained through a fitting procedure of the time spectrum for positrons having stopped in the MgO powder. These data are described by a sum of four exponential functions convoluted with the phenomenological response function $F(t)$ obtained through the measurements and analysis discussed in Section 3.1,

$$N_{\uparrow\downarrow}^{\pm}(t) = \left[\frac{n_0}{\tau_0} e^{-(t-t_0)/\tau_0} + \frac{n_{\text{PI}}}{\tau_{\text{PI}}} e^{-(t-t_0)/\tau_{\text{PI}}} + \frac{n_{\text{PT}}}{\tau_{\text{PT}}} e^{-(t-t_0)/\tau_{\text{PT}}} + \frac{n_{\text{T}}}{\tau_{\text{T}}} e^{-(t-t_0)/\tau_{\text{T}}} \right]_{\uparrow\downarrow}^{\pm} \otimes F_{\uparrow\downarrow}^{\pm}(t - t_0 + \Delta t_0). \quad (14)$$

Here, n_{PT} (respectively τ_{PT}) and n_{T} (respectively τ_{T}) are the amplitudes (respectively lifetimes) of the pseudo-triplet and of the triplet components, n_{PI} (respectively τ_{PI}) the amplitude (respectively lifetime) of the plastic component arising from positrons having stopped in the plastic start-detector, and n_0 (respectively τ_0) the amplitude (respectively lifetime) of the component matching the prompt peak. This last component includes both the pseudo-singlet short component (≈ 0.125 ns) and direct positron annihilation. The upper indices $+$ and $-$ refer to the direction of ^{12}N polarization, while \uparrow (respectively \downarrow) means that the magnetic field is antiparallel (respectively parallel) to the target-to-polarimeter direction. The function $F(t)$ is the time response function and was determined for the four conditions of the experiment, Δt_0 being the $t = 0$ time difference between the aluminum response function and the MgO data.

Since N^+ and N^- were measured “simultaneously”, all their respective components have the same lifetimes. Both N^+ and N^- were then fitted simultaneously with common lifetimes but different amplitudes. A simultaneous fit of N^+ and N^- then has 14 parameters: 4 common lifetimes, 8 amplitudes and 2 Δt_0 time differences. The fraction of positrons stopped in the plastic and their lifetime were taken to be the same for the MgO and the Al dump data. All the other 11 parameters were left free. The two relevant parameters are the two normalized pseudo-triplet amplitudes $\mathcal{N}_{\text{PT}}^+$ and $\mathcal{N}_{\text{PT}}^-$ — to be defined presently — or, more precisely, the normalized $\mathcal{N}_{\text{PT}}^+$ quantity and the ratio $r_{\text{PT}} = \mathcal{N}_{\text{PT}}^- / \mathcal{N}_{\text{PT}}^+$.

3.3.1. Normalization of the pseudo-triplet amplitude

In principle, four different types of normalization can be chosen: the pseudo-triplet component can be normalized to the triplet contribution (n_{TR}), to the total ($n_0 + n_{\text{PT}} + n_{\text{TR}}$), to the total without the triplet ($n_0 + n_{\text{PT}}$), or to the prompt peak (n_0). In the normalization to (n_0), the pseudo-singlet component which is also sensitive to the longitudinal polarization, has been taken into account. The normalization to the triplet has some disadvantages: it has lower statistics and the signal to noise (accidental events before subtraction) ratio is a factor ~ 100 times less favorable than for the normalizations with respect to $n_0 + n_{\text{PT}}$ or n_0 . Due to this poor signal to noise ratio, the triplet is more sensitive to a systematic error arising from the accidental subtraction, and, in addition, the determination of its amplitude

is more sensitive to the statistics of the response function due to its long after-pulse components. For these reasons a normalization to the triplet contribution was rejected. The two remaining types of normalization (to $n_0 + n_{PT}$ or to n_0) give equivalent results. Further discussion concerning systematic effects is presented in Section 5 and summarized in Table 3.

4. Results

A representative fit is shown in Fig. 5. Typical values for the parameters are

$$\tau_0 \sim 0.2 \text{ ns}, \quad \tau_{PT} \sim 7.48 \text{ ns}, \quad \tau_{TR} \sim 123 \text{ ns}, \quad \Delta t_0 \sim 10^{-2} \text{ ns},$$

and the triplet amplitude, normalized to $n_0 + n_{PT}$, is typically 0.28.

4.1. The analyzing power

As mentioned in Section 2.2, the analyzing power of the polarimeter is about $\epsilon = 0.25$ for a magnetic field of 9.3 kG. The quantity of interest to us however, is the effective analyzing power ϵP^+ , with P^+ the residual positron polarization projected onto the local magnetic field at the location where they are stopped and form positronium. The value for P^+ was computed to suffer a reduction from 1 to about 0.4 as a consequence of the geometrical acceptance of the spectrometer, of the precession of the positron spin in flight

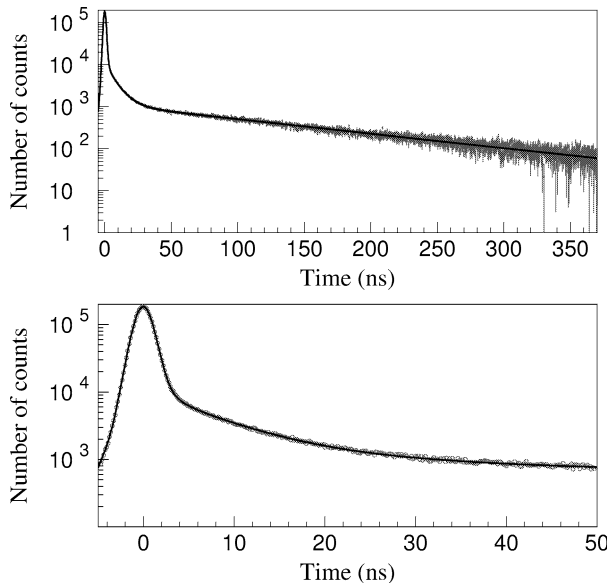


Fig. 5. Typical fit of an annihilation time spectrum in MgO to the theoretical $N(t)$ function defined in (14). The upper graph shows the complete fit interval, from -5 ns to 373 ns. The lower graph shows a zoom onto the -5 ns to 50 ns region. The quality of the fit is displayed in Fig. 6. This spectrum corresponds to two hours of data taking.

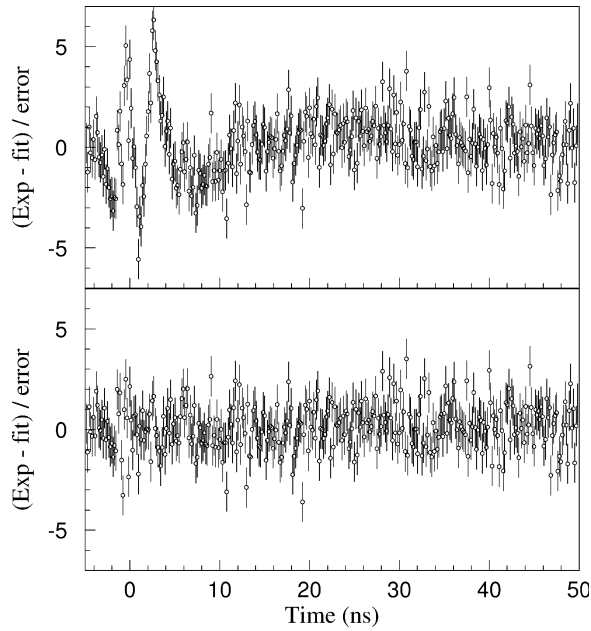


Fig. 6. The upper graph displays the quantity $(\text{exp}(t) - N(t))/\sigma_{\text{exp}(t)} \pm 1$, where $\text{exp}(t)$ stands for the experimental data and $N(t)$ is the theoretical function given in (14), for the fit presented in Fig. 5. One clearly distinguishes a structure in the prompt peak region ($\chi^2/\text{d.o.f.} = 1.15$). The lower graph shows the same plot with the peak being this time described by two short exponentials ($\chi^2/\text{d.o.f.} = 1.08$). The lifetime of the additional exponential is about 1 ns and its intensity is close to $\sim 2\%$. Physically, this exponential could be the signature of positronium formation at the MgO grain surface [27,28]. Several authors have found such short lived low intensity components in MgO [18,26]. If one chooses to describe the data by a sum of five exponentials, the final result for P^-/P^+ changes only by 5×10^{-5} (see Table 3).

and, most importantly, of positron depolarization due to Coulomb scattering in the MgO slowing down medium [25].

The normalized pseudo-triplet amplitudes are used to estimate the effective analyzing power, i.e. the product ϵP^+ of interest. These amplitudes can be expressed as functions of the positronium effective formation fraction f and the product ϵP^+ :

$$\mathcal{N}_{\text{PT}}^+ = \left(\frac{n_{\text{PT}}}{n_0 + n_{\text{PT}}} \right)_{\uparrow\downarrow}^+ = \frac{\frac{1}{4} f_{\uparrow\downarrow}^+ (1 \pm \epsilon P^+)}{1 - \frac{1}{2} f_{\uparrow\downarrow}^+}. \tag{15}$$

According to (15), the product ϵP^+ can be deduced from the asymmetry in the pseudo-triplet component which is induced by the magnetic field reversal indicated by the \uparrow and \downarrow symbols, only under the assumption that $f_{\uparrow}^+ = f_{\downarrow}^+$ which needs to be checked. In Section 5, it is effectively shown that the physical formation fraction is independent of both nuclear polarization orientations: $f^+ = f^-$. On the other hand, since the polarimeter field reversal also requires small relocations of the BaF₂ detectors and threshold readjustments, we were not able to reproduce exactly the same effective formation fraction for both magnetic field orientations: $f_{\uparrow} \neq f_{\downarrow}$.

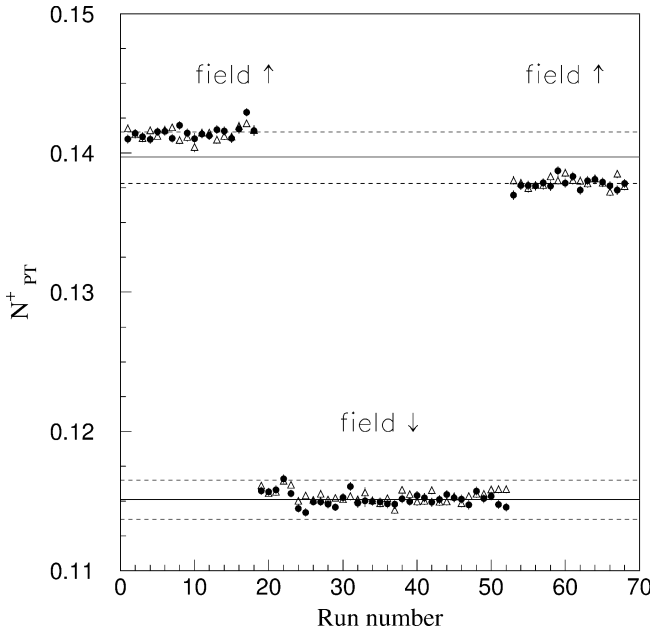


Fig. 7. The pseudo-triplet population \mathcal{N}_{PT}^+ normalized to $n_0 + n_{PT}$. The dashed lines correspond to the modification in the pseudo-triplet amplitude due to a $\pm 1.0 \times 10^{-2}$ variation in f . The horizontal axis displays the run number and each point corresponds to approximately 2 hours of data taking. Filled dots refer to events in window-A and open triangles to events in window-B.

The normalized pseudo-triplet amplitudes are shown for each file in Fig. 7. The two data sets taken with the \uparrow magnetic field direction are not in good agreement with one another. The reason for this difference may be either a change in the value for ϵ due to a modification of the magnetic field, or a change in the effective positronium formation fraction. Since the pseudo-triplet lifetime strongly depends on the magnetic field intensity and since for each polarimeter field orientation the pseudo-triplet lifetime was found to be identical, the first hypothesis has absolutely to be excluded. The difference between the two pseudo-triplet sets is compatible with a 1.0×10^{-2} change in the effective positronium formation fraction occurring when the field was reversed. In order to take into account this possible change in f due to the magnetic field reversal procedure, one has to assign to ϵP^+ an error by external consistency and assume an uncertainty for the pseudo-triplet populations associated to each magnetic field direction which corresponds to a 1.0×10^{-2} uncertainty on f . This latter uncertainty dominates the error on the product ϵP^+ and (15) then yields

$$\epsilon P^+ = (9.7 \pm 0.9) \times 10^{-2} \quad \text{with} \quad f_{\uparrow} = f_{\downarrow} = 0.40 \pm 0.01. \quad (16)$$

4.2. Ratio of the normalized pseudo-triplet populations, $(\mathcal{N}_{PT}^-/\mathcal{N}_{PT}^+)$

The ratio of the normalized pseudo-triplet amplitudes \mathcal{N}_{PT} is displayed for each file in Fig. 8, with the error bars reflecting only the statistics of the MgO data. Each measured

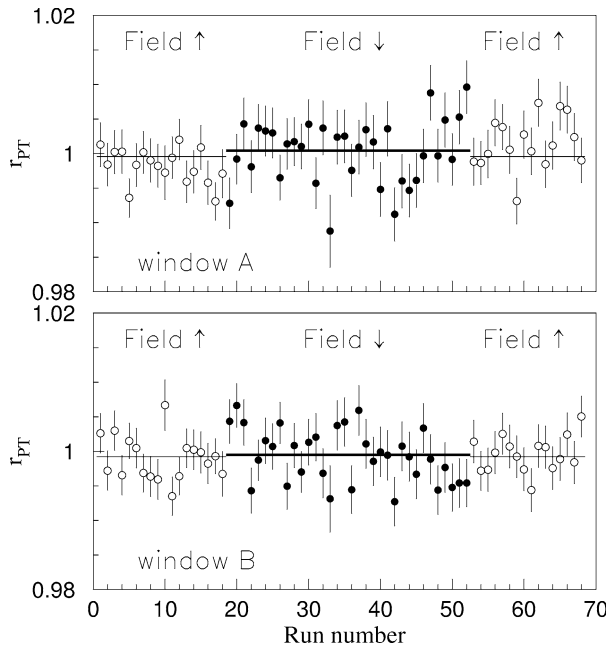


Fig. 8. Ratio of the normalized pseudo-triplet amplitudes for both A and B windows. Results are displayed in chronological order.

Table 2

Window	$(r_{PT})_{\uparrow}$	$(\sigma_r)_{\uparrow}$	$(\chi^2/\nu)_{\uparrow}$	$(r_{PT})_{\downarrow}$	$(\sigma_r)_{\downarrow}$	$(\chi^2/\nu)_{\downarrow}$
A	0.99955	0.00056	1.18	1.00040	0.00065	1.39
B	0.99921	0.00051	1.18	1.00044	0.00059	1.26

response function was used to fit those sets of the MgO data which preceded or were subsequent to its measurement. A fit by a constant of the ratio $r_{PT} = (\mathcal{N}_{PT}^-/\mathcal{N}_{PT}^+)$ with each term normalized to $(n_{PT} + n_0)$ was made separately for each magnetic field orientation, giving the results as in Table 2.

In order to take into account the nonstatistical fluctuations of the response functions, the errors quoted above were increased by multiplying each by the square root of the normalized χ^2 . Defining a superratio as

$$S \stackrel{\text{def}}{=} \frac{(\mathcal{N}_{PT}^-/\mathcal{N}_{PT}^+)_{\uparrow}}{(\mathcal{N}_{PT}^-/\mathcal{N}_{PT}^+)_{\downarrow}}, \tag{17}$$

one then finds $S = 0.99915 \pm 0.00098$ for window-A and $S = 0.99969 \pm 0.00084$ for window-B. Given the relation

$$S = 1 - 2\epsilon P^+ \left(1 - \frac{P^-}{P^+}\right), \tag{18}$$

the value for the product ϵP^+ in Section 4.1, and identical f 's, we finally have

$$\frac{P^-}{P^+} = 0.9957 \pm 0.0050 \text{ stat} \pm 0.0005 \text{ syst} \quad (\text{window-A}),$$

$$\frac{P^-}{P^+} = 0.9984 \pm 0.0043 \text{ stat} \pm 0.0002 \text{ syst} \quad (\text{window-B}). \quad (19)$$

The results obtained using the alternative normalization to n_0 with $f = 0.4$ are identical. At this stage, the systematic error only reflects the one introduced by the determination of the product ϵP^+ . The impact of further systematic errors is discussed in the next section.

5. Systematic errors and final result

The identified systematic errors and corrections are reported in Table 3. They are dominated by the uncertainty on the effective analyzing power ϵP^+ . As discussed in Section 4.1, this error was determined through external consistency by considering all pseudo-triplet amplitudes for the entire experiment (Fig. 7).

5.1. Instrumental effects

Eq. (18) which leads to the results (19) assumes that the probability to form and detect decays from the pseudo-triplet state is the same for the four different experimental conditions. The probability to detect pseudo-triplet decays relative to the normalization (peak + pseudo-triplet) depends slightly on the $3\gamma/2\gamma$ detection efficiency, since a small fraction (5%) of the pseudo-triplet decays are into 3γ 's and most of the normalization originates from 2γ events.

Table 3
Systematic errors and corrections to be applied to the ratio P^-/P^+

Sources of systematic errors	Systematic uncertainties and additive corrections
Analyzing power	$\pm 5 \times 10^{-4}$ A $\pm 2 \times 10^{-4}$ B
Instrumental effect	$\pm 1 \times 10^{-4}$
Analysis procedure	
τ_{Al}	$\pm 1.6 \times 10^{-4}$
n_{pl}	$\pm 2 \times 10^{-5}$
$\frac{(n_{pl})_{\uparrow}}{(n_{pl})_{\downarrow}}$	-2×10^{-5}
τ_{pl}	$+(2 \pm 1) \times 10^{-4}$
Peak	$\pm 5 \times 10^{-5}$
Unpolarized background	$\pm 1.2 \times 10^{-5}$ A $\pm 3.4 \times 10^{-5}$ B
Accidentals subtraction	$\pm 9 \times 10^{-5}$
^{12}N decay branch to 4.4 MeV	-8.5×10^{-5}
Total	$+1 \pm 6 \times 10^{-4}$ A $+1 \pm 3 \times 10^{-4}$ B

In principle both the effective positronium formation fraction f and the $3\gamma/2\gamma$ relative detection efficiency g may change with the target spin or field reversal.

Assuming that f and g differ for all four different experimental conditions, (18) becomes

$$S \approx 1 - 2\epsilon P^+ \left(1 - \frac{P^-}{P^+}\right) + 0.05(b - 1) + 1.25(a - 1), \quad \text{where} \quad (20)$$

$$a = \frac{(f^-/f^+)_{\uparrow}}{(f^-/f^+)_{\downarrow}}, \quad b = \frac{(g^-/g^+)_{\uparrow}}{(g^-/g^+)_{\downarrow}}. \quad (21)$$

As one can see from the above equation, thanks to the relative character of the present experiment and to the field inversion, the measurement may only be affected by the superratios of f and g . The consequence of this is that the change of f with field reversal discussed in Section 4 has no influence on the result if f is independent of the target polarization state. In the same way, a change of f correlated with target spin reversal will cancel in the superratio if this correlation is independent of the polarimeter field orientation. The same applies to g .

Both factors a and b entering in (20) were determined experimentally. The intrinsic positronium formation fraction is the same for the different experimental conditions. The only factor that may affect the effective positronium formation fraction f^- to be different from f^+ is a displacement of the proton beam and of the ^{12}N activity, resulting in a modification of the positron stopping region. The parameter a was measured by monitoring the beam position and the associated change in f , leading to $|(a - 1)| < 1.6 \times 10^{-5}$.

The $3\gamma/2\gamma$ detection efficiency may be affected by a shift in the threshold induced by the change in event rate under target spin flip. Threshold variations were continuously monitored through γ amplitude spectra accumulated in parallel with time spectra, leading to $b - 1 = (1.0 \pm 2.1) \times 10^{-4}$ in window-A and $b - 1 = -(1.3 \pm 1.5) \times 10^{-4}$ in window-B.

These two possible instrumental effects lead to a systematic uncertainty of 1.0×10^{-4} on the polarization ratio as shown in Table 3.

5.2. Effects introduced by the analyzing procedure

As described in Section 3, some parameters had to be fixed in the adjustment used to extract the amplitude of the relevant positronium annihilation time components.

As mentioned in Section 3.1, the determination of the detector's time response function using the annihilation of positrons in aluminum has to account for the finite lifetime of free positrons in aluminum. This lifetime was taken to be 250 ps [18]. The scatter of reported lifetimes is from 150 ps to 290 ps [18]. Taking the extreme value of 150 ps would modify our result by a negligible amount of -1.6×10^{-4} only. This difference is considered as a systematic error and is reported in Table 3.

The adjustment also had to take into account the annihilation spectrum of the positrons which stopped in the plastic start-detector. The relative amplitude of the "plastic component" was determined in the manner explained in Section 3.2. If this relative

amplitude is — conservatively — modified by a factor two, this has still a negligible impact of 2×10^{-5} , as indicated in Table 3. Furthermore, the analysis assumed that the “plastic component” was identical for both directions of the magnetic field. Moreover, if one takes into account the small analyzing power for positrons stopped in the stop-detector, a Monte-Carlo evaluation establishes that this has a negligible impact of -2×10^{-5} on our result. In the analysis, the lifetime of positronium in plastic was assumed to be 2 ns [26]. Using our own experimental value of 1.85 ± 0.08 ns which provides the best fit to our data, our result changes by $(2 \pm 1) \times 10^{-4}$.

The adjustment described in Section 3.3 provides a globally satisfactory normalized χ^2 of 1.15 but has shortcomings in the peak region as shown in the upper part of Fig. 6. This anomaly can be removed, resulting only in a slightly improved global χ^2 of 1.08 as shown in the lower part of Fig. 6, by assuming the existence of a second pseudo-triplet component (2%, lifetime 1 ns). Such anomalies have been reported previously in the literature [18,26] and attributed to positrons stopping on the surface of the MgO grains [27,28]. If this were the case, the analyzing power of this component would be identical to that of the dominant pseudo-triplet one. The impact of such an additional component on our result is 5×10^{-5} .

5.3. Impact of a long lived background activity

A long lived activity of unknown origin was noticed in the time spectra. In an ancillary measurement which used long measuring cycles, the lifetime of this activity was larger than 100 ms. Furthermore, its contribution to our data was evaluated to be $3.92 \pm 0.11\%$ in the A-window and $11.12 \pm 0.34\%$ in the B-window.

This long-lived component did not display any β asymmetry, hence the emitting nucleus is unpolarized. Considering existing limits on possible right-handed currents, it may thus be assumed that the polarization of the spurious positrons equals their velocity, i.e. with a range of β values lying within 0.989 and 1.0.

Using this information, the systematic error induced by this spurious activity on our result is 1.2×10^{-5} in window-A and 3.4×10^{-5} in window-B.

5.4. Impact of the ^{12}N decay branch feeding the 4.44 MeV 2^+ excited level of ^{12}C

A 1.9% decay branch feeds the 4.44 MeV 2^+ excited level of ^{12}C . Considering the settings of our spectrometer, the contribution of that level to our data equals 3%.

To estimate the effect introduced by this contribution, let us assume a pure V–A interaction. Given this assumption as well as the polarization and spectrometric characteristics of our device, the ratio P^-/P^+ for this branch is 1.00285 times larger than the one for our main transition.

The corresponding correction reduces our result by 8.5×10^{-5} .

5.5. Accidental positron–photon coincidences

This contribution to time spectra arises from stop signals which are not due to the annihilation of the positrons which triggered the start-detector. These accidental

coincidences within the 500 ns photon observation window are of two types. They may be due either to stop signals generated by the general photon background, or to photons originating from the annihilation of a positron different from the one which triggered the start-detector.

The accidentals of the first type can be measured at “the left” of the direct annihilation peak in the time spectra, i.e. by considering the photons which preceded the arrival of the positron. Extrapolating this value to the “right”, i.e. to the region of interest to the experiment, one took into account the probability that a real annihilation photon preceded the accidental one which, of course, is then absent. The accidentals of the second type were evaluated on the basis of count rates recorded in various scalers. Computational details for both types of subtractions can be found in [8].

The propagation of the statistical errors which enter the determination of the accidental contribution results in a systematic error of $\pm 9 \times 10^{-5}$ on the result, as indicated in Table 3. It should be stressed that by normalizing our data to the triplet component, in which case the number of accidentals is comparable to that of the real events, would not push our result outside of this error bar.

Table 3 also shows the quadratically combined sum of all corrections and of all systematic errors discussed in this section both for windows A and B.

5.6. Final result

Considering the results of the fits discussed in Section 4 and the systematic corrections and errors discussed in this section, we finally obtain the following values:

$$\begin{aligned}
 R &= \frac{P^-}{P^+} = 0.9958 \pm 0.0050 \text{ stat} \pm 0.0006 \text{ syst} \quad (\text{window-A}), \\
 R &= \frac{P^-}{P^+} = 0.9985 \pm 0.0043 \text{ stat} \pm 0.0003 \text{ syst} \quad (\text{window-B}), \\
 R &= \frac{P^-}{P^+} = 0.9974 \pm 0.0033 \text{ stat} \pm 0.0006 \text{ syst} \quad (\text{weighted mean A and B}), \quad (22)
 \end{aligned}$$

and, using (3) and (11),

$$\begin{aligned}
 \Delta &= 0.0008 \pm 0.0045 \text{ stat} \pm 0.0005 \text{ syst} \quad (\text{window-A}), \\
 \Delta &= -0.0016 \pm 0.0041 \text{ stat} \pm 0.0003 \text{ syst} \quad (\text{window-B}), \\
 \Delta &= -0.0005 \pm 0.0030 \text{ stat} \pm 0.0005 \text{ syst} \quad (\text{weighted mean A and B}). \quad (23)
 \end{aligned}$$

It should be stressed that the results obtained in the two measuring windows are independent. They correspond to different source activities, so that their agreement gives us confidence that no rate dependent systematic effects were overlooked.

It should also be emphasized that a normalization to the peak region only would give results identical to those reported above within the quoted digits.

6. Implications of the result for physics beyond the Standard Model and confrontation with similar constraints

6.1. Introduction

The present experiment being the measurement of a helicity observable of nuclear beta-decay, is sensitive to any deviation from the Standard Model which affects the helicity of the decay products. Many such scenarios have been discussed in the literature, for instance the interplay of exotic fermions, the exchange of charged Higgs bosons, that of supersymmetric sleptons or even leptoquarks [29]. There is also considerable interest in scenarios which introduce a right-handed gauge boson in addition to the standard left-handed one, recovering parity symmetry at some large energy scale [30]. Here, we shall more specifically illustrate the impact of our experiment in constraining right-handed gauge bosons.

For ease of reference, let us recall the classic most general four-fermion effective interaction Hamiltonian parametrized in terms of effective nucleonic coupling constants C_i [31],¹⁰

$$H_{\text{eff}}^{\text{nucl}} = \bar{\psi}_p \gamma_\mu \psi_n \bar{\psi}_e (C_V \gamma^\mu - C'_V \gamma^\mu \gamma_5) \psi_{\nu_e} - \bar{\psi}_p \gamma_\mu \gamma_5 \psi_n \bar{\psi}_e (C_A \gamma^\mu \gamma_5 - C'_A \gamma^\mu) \psi_{\nu_e} \\ + \frac{1}{2} \bar{\psi}_p \sigma_{\lambda\mu} \psi_n \bar{\psi}_e (C_T \sigma^{\lambda\mu} - C'_T \sigma^{\lambda\mu} \gamma_5) \psi_{\nu_e} + \bar{\psi}_p \psi_n \bar{\psi}_e (C_S - C'_S \gamma_5) \psi_{\nu_e} \\ + \bar{\psi}_p \gamma_5 \psi_n \bar{\psi}_e (C_P \gamma_5 - C'_P) \psi_{\nu_e} + \text{H.c.} \quad (24)$$

In the Standard Model, one has

$$C_A = C'_A, \quad C_V = C'_V \quad (25)$$

as well as

$$C_T = C'_T = C_S = C'_S = C_P = C'_P = 0, \quad (26)$$

with the coupling coefficients C_V and C_A related to the tree-level $SU(2)_L$ gauge coupling constant g and the left-handed gauge boson mass M_W by

$$\frac{C_A}{g_A} = \frac{C_V}{g_V} = \frac{g^2}{8M_W^2} V_{ud}, \quad (27)$$

g_A and g_V being the nucleonic axial and vector electroweak form factors at zero momentum transfer and V_{ud} the (u, d) element of the Cabibbo–Kobayashi–Maskawa flavour mixing matrix.

In the case of the pure Gamow–Teller transition at hand, only the coupling coefficients C_A , C'_A , C_T and C'_T contribute in the allowed approximation. The expression for Δ is then given by [7]:

$$\Delta = \frac{|C_A - C'_A|^2}{|C_A + C'_A|^2} \frac{1}{\left[1 - \frac{|C_A - C'_A|^2}{|C_A + C'_A|^2}\right]^2}. \quad (28)$$

¹⁰ Compared to that of Refs. [19,21], our sign convention for these coupling coefficients is adapted in order that the left-handed chiral projector $(1 - \gamma_5)/2$ agrees with the modern choice of sign for γ_5 [32], while still preserving the expressions for correlations functions as given in Refs. [19,21].

6.2. Constraint on right-handed currents

As mentioned above, left–right symmetric models were introduced [33–35] to restore left–right symmetry at a fundamental level with maximal parity violation being a low-energy property only due to spontaneous symmetry breaking in the gauge sector. In its simplest form based on the $SU(2)_L \times SU(2)_R \times U(1)_{B-L}$ gauge group, the model introduces in addition to the known charged gauge boson of mass $M_1 = 80.42 \text{ GeV}/c^2$ a heavier one whose mass we shall denote as M_2 with $\delta = (M_1/M_2)^2$. Assuming time reversal invariance, these two physically observable charged gauge bosons W_1 and W_2 couple to fermions of left- and right-chirality according to the mixing of the basic $SU(2)_L$ and $SU(2)_R$ charged gauge bosons W_L and W_R ,

$$W_L = W_1 \cos \zeta + W_2 \sin \zeta, \quad (29)$$

$$W_R = -W_1 \sin \zeta + W_2 \cos \zeta. \quad (30)$$

First, let us consider the constraints provided by the present experiment for the “manifest” left–right symmetric model which introduces only these two parameters δ and ζ , and compare these constraints to those set by other experiments.

6.2.1. Manifest left–right symmetric model: experimental constraints from nuclear beta-decay

Within this two parameter model, the quantity Δ to which our experiment is sensitive then reduces to

$$\Delta = (\delta + \zeta)^2, \quad (31)$$

so that the experimental result (23) directly translates into

$$(\delta + \zeta)^2 = -0.0005 \pm 0.0030. \quad (32)$$

In the particular case that $\zeta = 0$, and using the value $M_{W_1} = 80.42 \pm 0.06 \text{ GeV}/c^2$, our experiment sets the following lower bound on the mass of a hypothetical right-handed gauge boson W_2 ,

$$M_{W_R} > 310 \text{ GeV}/c^2 \quad 90\% \text{ CL}. \quad (33)$$

Combining this limit with those obtained previously in ^{12}N [4] and ^{107}In [5], a more stringent constraint is set, namely $(\delta + \zeta)^2 = -0.0004 \pm 0.0026$ (world average), which again in the case that $\zeta = 0$ leads to a comparable lower bound on the mass of a right-handed gauge boson.

It is interesting to combine the world average results of these polarization measurements with those of other experiments in nuclear beta-decay. The latter are essentially of two types: (1) relative measurements of β -polarizations in Fermi and Gamow–Teller decays P_F/P_{GT} , and (2) beta- and neutrino-asymmetry measurements in neutron-decay combined with the neutron ft -value. The combination of all these experiments, whose constraints are represented individually in Fig. 9, provides the 90% CL exclusion-plot in the (δ, ζ) plane displayed in Fig. 10. This figure represents the expression

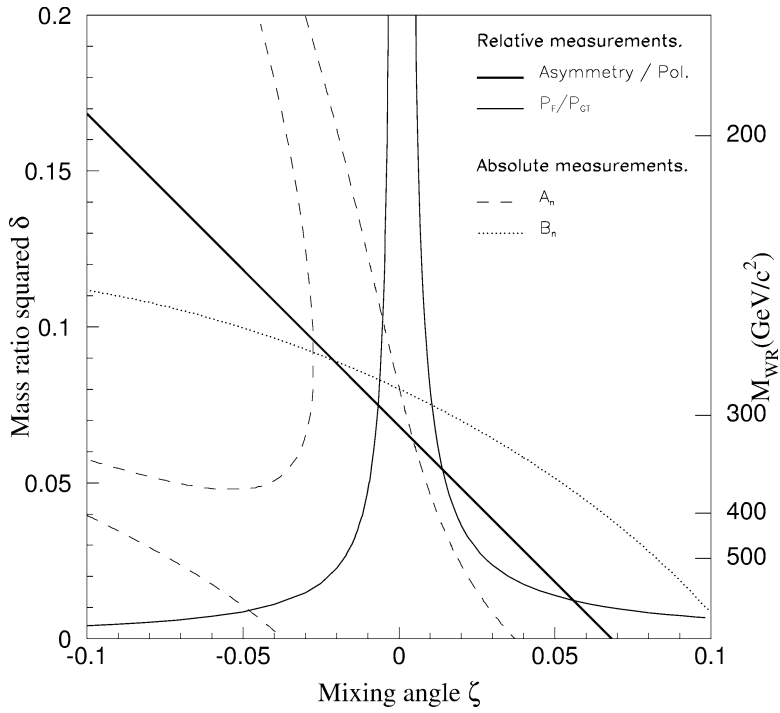


Fig. 9. The 90% confidence limit constraints provided by the individual nuclear β -decay experiments discussed in Section 6.2.1. The allowed regions are those containing $(\delta, \zeta) = (0, 0)$.

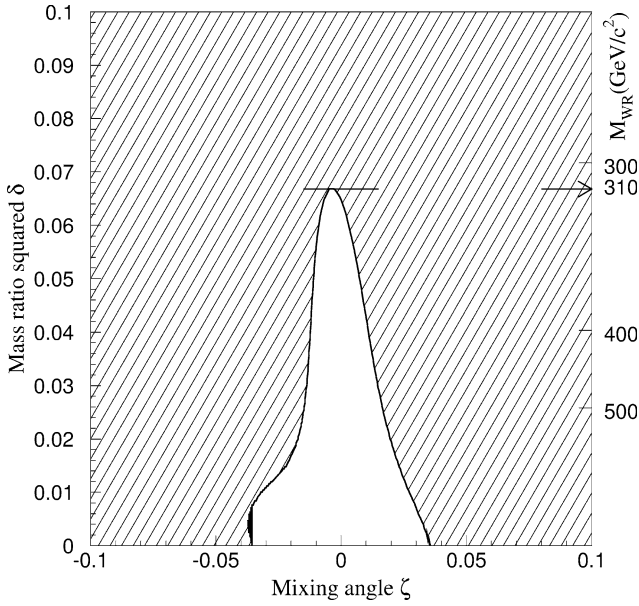


Fig. 10. Exclusion plot in the (δ, ζ) plane from all existing β -decay experiments.

$$\begin{aligned} & [\Delta_{\text{exp}} - \Delta_{\text{th}}(\zeta, \delta)]^2 + \left[\left(\frac{P_{\text{F}}}{P_{\text{GT}}} \right)_{\text{exp}} - \left(\frac{P_{\text{F}}}{P_{\text{GT}}} \right)_{\text{th}}(\zeta, \delta) \right]^2 + \Sigma_{a,b} [O_{\text{n}} - O_{\text{nth}}(\zeta, \delta)]^2 \\ & = \chi_{\text{min}}^2 + 1, \end{aligned} \quad (34)$$

where $\Delta = -0.0004 \pm 0.0026$ is the aforementioned world average of asymmetry-polarization experiments dominated by the one reported here, $P_{\text{F}}/P_{\text{G}} = 1 + 8\delta\zeta = 1.0010 \pm 0.0027$ [36,37] combined with the limit of Ref. [38], and O_{n} is the combination of the relevant neutron decay results. The latest world average values were used, namely $O_{\text{a}} = A_{\text{n}} = -0.1174 \pm 0.0011$ [39],¹¹ $O_{\text{b}} = B_{\text{n}} = 0.983 \pm 0.004$ [40]. For the reduced transition probabilities, the values $ft_{\text{n}} = 1052.3 \pm 1.4$ [41] and $ft_{0^+ \rightarrow 0^+} = 3072.3 \pm 2.0$ [42] were used.

6.2.2. Manifest left–right symmetric models: constraints from other sources

Neutrinoless double-beta decay sets a lower bound of $2 \text{ TeV}/c^2$ on the right-handed gauge boson mass [43,44], provided that the right-handed neutrino is heavy, which, however, is not a scenario to which our experiment is sensitive. If the right-handed neutrino mass moves down into the keV region or less, where it could affect beta-decay observables, the mass limit extracted from neutrinoless double beta-decay limits disappears [45].

The experiment [46] having measured the positron asymmetry in muon decay yields a lower bound of $M_{\text{WR}} > 420 \text{ GeV}/c^2$. However, this experiment consisted in an absolute measurement without the advantage of any enhancement effect, in contradistinction to asymmetry polarization correlation measurements, while it also suffered systematic effects at the corresponding precision level [46]. Furthermore, the mass constraint on a possible right-handed gauge boson stemming from this experiment has to assume a rather light right-handed muon neutrino [46].

The $K_{\text{S}}\text{--}K_{\text{L}}$ mass difference also provides [47], in manifest left–right symmetric models, a lower bound of $M_{\text{WR}} > 1.6 \text{ TeV}/c^2$ [48]. This limit could possibly be weakened by accidental cancellations between the dominant contributions and those of additional Higgs particles (e.g. bi-doublets) which are in any case required in left–right symmetric extensions of the Standard Model [49], although this scenario has not been explored in any detail so far. Finally, let us note that a vanishing lower bound on M_{WR} due to accidental cancellations in this purely hadronic observable has been addressed in generalized left–right symmetric models that allow for different Cabibbo–Kobayashi–Maskawa matrix elements in their left- and right-handed chiral sectors [45]. Such models are discussed in the next section.

As mentioned previously, stringent lower bounds on extra gauge bosons follow from $p\text{--}\bar{p}$ collider searches through the production of energetic charged leptons at large transverse momentum [50,51]. It has been pointed out that these constraints may not hold considering the possible decay of the $p\text{--}\bar{p}$ produced right-handed gauge boson into a pair of Higgs particles which are in any case required by any left–right symmetric extension of the Standard Model [52]. However, since these additional Higgs particles

¹¹ Errors were inflated in order to account for the scatter in the data.

would have to possess in this case a rather small mass, they seem to be excluded already through the K_S-K_L mass difference unless one allows for fine tuned accidental cancellations [53]. However, as shall be discussed in the following section, for generalized left–right symmetric models the collider constraints prove to be complementary to those stemming from nuclear beta-decay experiments.

6.2.3. Complementarity of our experiment in generalized left–right symmetric models

The parameter space of generalized left–right symmetric models [54] is enlarged by allowing for different $SU(2)_L$ and $SU(2)_R$ gauge coupling constants g_L and g_R , $r_g = g_R/g_L \neq 1$, for different Cabibbo–Kobayashi–Maskawa matrix elements V_{ud}^L and V_{ud}^R , and for different neutrino mixing matrix elements in both sectors, since neutrinos are typically massive in such models. For further purposes, let us thus introduce the following quantities:

$$v_{LL} = V_{ud}^L U_{ie}^{L*}, \quad v_{LR} = V_{ud}^L U_{ie}^{R*}, \quad v_{RL} = V_{ud}^R U_{ie}^{L*}, \quad v_{RR} = V_{ud}^R U_{ie}^{R*}, \quad (35)$$

$$v'_{LL} = V_{ud}^L \sqrt{u^L}, \quad v'_{LR} = V_{ud}^L \sqrt{u^R}, \quad v'_{RL} = V_{ud}^R \sqrt{u^L}, \quad v'_{RR} = V_{ud}^R \sqrt{u^R}, \quad (36)$$

$$u^L = \sum_i |U_{ie}^L|^2 \quad \text{and} \quad u^R = \sum_i |U_{ie}^R|^2, \quad (37)$$

where U_{ie}^R and U_{ie}^L are the right- and left-handed neutrino mixing matrices. Primed quantities refer to the fact that the summation is performed only over those massive neutrino states whose production is kinematically allowed, while also absorbing into these quantities the possibly ensuing phase-space reduction factors.

Furthermore, let us also adopt the following notations [54,55]:

$$\begin{aligned} \eta'_{LL} &= \eta_0 v'_{LL} (1 + \delta t^2), & \eta'_{LR} &= -\eta_0 v'_{LR} r_g t (1 - \delta), \\ \eta'_{RL} &= -\eta_0 v'_{RL} r_g t (1 - \delta), & \eta'_{RR} &= \eta_0 v'_{RR} r_g^2 (t^2 + \delta), \end{aligned} \quad (38)$$

$$\text{with } \eta_0 = \frac{1}{M_1^2} \left(\frac{g_L^2}{8} \right) \cos^2 \zeta \quad \text{and} \quad t = \tan \zeta. \quad (39)$$

The quantity Δ to which our experiment is sensitive, with its experimental value given in (23), may then be expressed as

$$\Delta = \frac{|\eta'_{RR} - \eta'_{LR}|^2}{|\eta'_{LL} - \eta'_{RL}|^2} \frac{1}{\left[1 - \frac{|\eta'_{RR} - \eta'_{LR}|^2}{|\eta'_{LL} - \eta'_{RL}|^2} \right]^2}. \quad (40)$$

Since the impact of a massive neutrino sector and the influence of the generalized scenarios on the K_S-K_L mass difference have already been mentioned previously, let us address here only the complementarity of our limits to those deduced from collider experiments.

For ease of discussion, let us turn on one by one only each of the parameters of the generalized models by giving them a value different from those they have in the Standard Model. Moreover, the possibility of neutrino mixing shall be ignored. Although mixing of small mass neutrino eigenstates has now been observed [56], we are unaware of extensions of this observation to the right-handed sector.

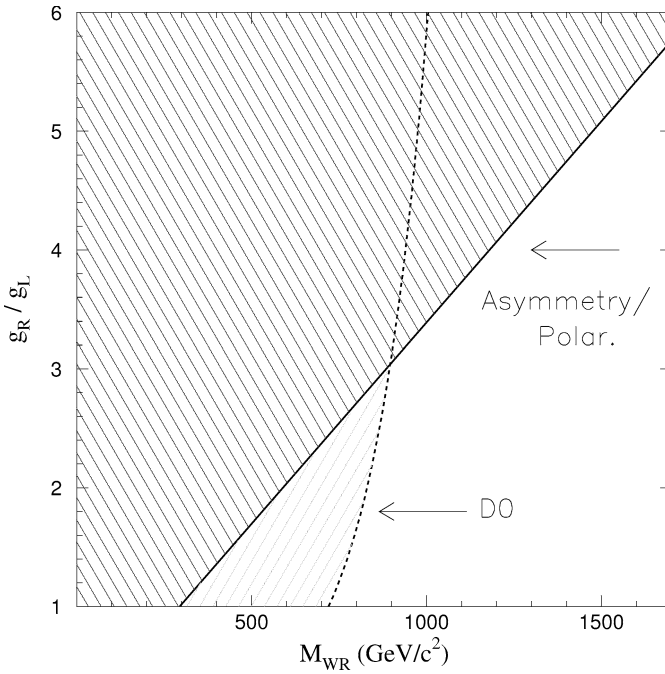


Fig. 11. Limits on a right-handed gauge boson mass as a function of the g_R/g_L ratio, showing the complementarity between our experiment and the D0 one. The value $\zeta = 0$ is assumed.

As remarked by P. Herczeg [57], the collider constraints limit the product of the production cross-section of an extra W-boson with its leptonic branching ratio, which provides a combination of parameters different from that in beta-decay or muon-decay observables [55,58]. Fig. 11 illustrates the effect which follows from this different dependency on parameters in the limit that $\zeta = 0$ and assuming identical values for the Cabibbo–Kobayashi–Maskawa matrix elements of the two chiral sectors, while keeping the ratio of gauge coupling constants different from unity, $r_g = g_R/g_L$. As that figure shows, for a ratio r_g larger than 3, beta-decay experiments become complementary to collider ones in providing a lower bound on the mass of a hypothetical right-handed heavy gauge boson.

A similar conclusion may be drawn, still in the limit that $\zeta = 0$, for a scenario in which the gauge couplings are identical, $r_g = 1$, while Cabibbo–Kobayashi–Maskawa matrix elements differ in the two chiral sectors. In this case, as illustrated in Fig. 12, beta-decay experiments can exclude right-handed gauge bosons with a mass comparable to (or lower than) that of the known boson at $80 \text{ GeV}/c^2$. The maximal parity violation observed experimentally would then be attributed to the smallness of the corresponding matrix element V_{ud}^R . The consistency of this scenario with other constraints has yet to be explored [59].

A last comment with respect to complementarity with muon decay observables is in order. Nuclear beta-decay tests have to assume sufficiently light right-handed electron neutrinos. Since the same assumption must also be made for right-handed muon neutrinos

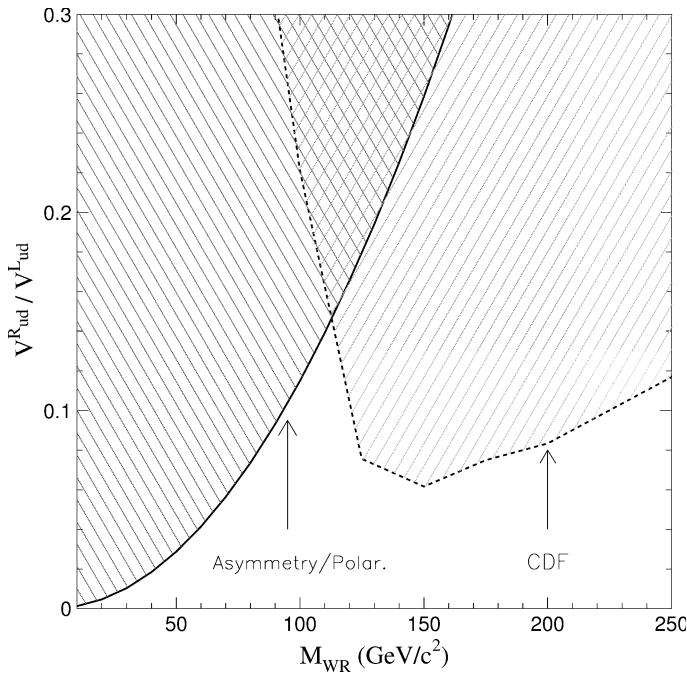


Fig. 12. Limits on a right-handed gauge boson mass as a function of the V_{ud}^R/V_{ud}^L ratio, illustrating the complementarity between our experiment and the CDF one. The value $\zeta = 0$ is assumed.

in the case of muon decay experiments, the two types of measurements are complementary. In this context, it should also be noted that an ongoing positron asymmetry-polarization experiment in muon decay [60] tests a different combination of the parameters in the right-handed neutrino sector [61], making these two classes of experiments complementary in the context of general left–right symmetric models.

7. Conclusions

This paper presents the results of a precision experiment measuring the polarization-asymmetry correlation of the positron longitudinal polarization in the β^+ -decay of ^{12}N , based on the considerations developed in Ref. [6] and improving on previous similar measurements [4,5,26]. The general principle lies with the relative measurement of the longitudinal polarizations for positrons emitted parallel and antiparallel to the nuclear spin orientation, this ratio being compared to the value expected within the Standard Model for the electroweak interaction. This observable is especially sensitive to any deviation away from the (V–A) structure of the electroweak charged current on two counts. For one of the relative emission directions, not only is the count rate in the (V–A) case vanishing but the positron polarization also opposite to what it ought to be for a pure (V–A) interaction.

The interest of such an enhanced sensitivity to a deviation from the Standard Model value is compounded further with the relative character of the measurement, implying

that a great many possible sources of systematic corrections affecting any absolute polarization measurement are disposed off at the outset. As has been discussed, the remaining systematic corrections are small and well under control, and affect the final result only to a small degree, whose evaluation is achieved with great confidence.

The positron polarimetry technique uses the well established method of time resolved positronium spectroscopy in an applied magnetic field, in which the pseudo-triplet contribution to the time decay spectrum carries the relevant positron polarization information. Detailed tests have been performed to cross check in as many ways as possible the reliability of the extracted relative positron polarizations with the required precision, due attention being paid to all imaginable instrumental effects incurred through the experimental set-up.

The achieved final result stands as one of the most stringent constraints to date for precision tests of the Standard Model in the realm of semileptonic weak nuclear processes. For a specific quantity Δ , whose definition is given in the body of the text (28) and which vanishes in the Standard Model, the experiment leads to the value

$$\Delta = -0.0005 \pm 0.0030 \text{ stat} \pm 0.0005 \text{ syst}, \quad (41)$$

thus in perfect agreement with the Standard Model. In turn, this result may be translated in terms of parameters of specific extensions for physics beyond that model. One among other scenarios of interest is that provided by so-called left–right symmetric models with their right-handed charged electroweak interactions. For instance, assuming a manifestly symmetric such model, as well as a vanishing mixing angle between the two species of charged massive gauge bosons, our experiment sets the lower bound

$$M_{W_R} > 310 \text{ GeV}/c^2 \quad 90\% \text{ CL}, \quad (42)$$

the most stringent constraint yet on the mass of such a right-handed gauge boson from any low-energy nuclear physics experiment. When relaxing some of the simplifying assumptions on which this limit is based, larger chunks of the parameter spaces of models beyond the Standard Model are thus explored, in ways complementary to other experiments whether at high energies or in the intermediate-energy muonic sector. Examples of such complementary constraints stemming from our measurement and other experiments at the $p\text{--}\bar{p}$ collider and in muon decay have also been provided.

Acknowledgements

We would like to thank Dr. P. Schmelzbach and his team at the Paul Scherrer Institute (Villigen, Switzerland) for driving the Phillips cyclotron with the highest proton polarization possible, as well as P. Demaret of the Institute of Nuclear Physics in Louvain-la-Neuve for the preparation of the stacked carbon–aluminum targets.

Appendix A. Evaluation of the corrections to R_0 and k due to spin rotation and inhomogeneity of the analyzing power (see Section 2.3.2)

In order to be specific, let us state with precision our notation for nuclear polarization. Nuclear polarization is defined with respect to a specific normalized direction in space pointing from the ^{12}N source to the polarimeter, and denoted by the unitary vector \hat{J} . The vector of ^{12}N nuclear polarization then has a component $-1 \leq J \leq +1$ along that \hat{J} axis, so that the actual nuclear polarization vector is given by $\vec{J} = J \hat{J}$. Eq. (10) then reads:

$$P(J\hat{J}) = \frac{1}{\langle 1 \rangle + JA\langle \beta(\hat{p} \cdot \hat{J}) \rangle + \left\langle \frac{m}{E} b \right\rangle} \times \langle \epsilon(\vec{r})\hat{n} \cdot \mathcal{R}[\beta G\hat{p} + NJ\hat{J} + Q^*J(\hat{p} \cdot \hat{J})\hat{p} + \beta RJ(\hat{p} \times \hat{J})] \rangle. \quad (43)$$

Introducing the definitions

$$b' = \left\langle \frac{m}{E} \right\rangle b, \quad (44)$$

$$\Lambda = \frac{\langle \beta(\hat{p} \cdot \hat{J}) \rangle}{\langle 1 \rangle}, \quad (45)$$

$$\Omega_1 = \frac{1}{\Lambda} \frac{\langle \epsilon(\vec{r})(N(\mathcal{R}\hat{J}) \cdot \hat{n} + Q^*(\hat{p} \cdot \hat{J})(\mathcal{R}\hat{p}) \cdot \hat{n}) \rangle}{\langle \epsilon(\vec{r})\beta(\mathcal{R}\hat{p}) \cdot \hat{n} \rangle}, \quad (46)$$

$$\Omega_2 = \frac{1}{\Lambda} \frac{\langle \epsilon(\vec{r})\beta R(\mathcal{R}(\hat{p} \times \hat{J})) \cdot \hat{n} \rangle}{\langle \epsilon(\vec{r})\beta(\mathcal{R}\hat{p}) \cdot \hat{n} \rangle}, \quad (47)$$

Eq. (43) acquires the form

$$P(J\hat{J}) \stackrel{\text{def}}{=} P(J) = \frac{\langle \epsilon(\vec{r})\beta(\mathcal{R}\hat{p}) \cdot \hat{n} \rangle}{\langle 1 \rangle} \frac{G + J\Lambda(\Omega_1 + \Omega_2)}{1 + AJ\Lambda + b'}. \quad (48)$$

From the expression for the decay rate,

$$N_{\beta\gamma}(J\hat{J}) \stackrel{\text{def}}{=} N_{\beta\gamma}(J) \propto \left(1 + JA\langle \beta(\hat{p} \cdot \hat{J}) \rangle + \left\langle \frac{m}{E} b \right\rangle \right), \quad (49)$$

the experimental β asymmetry A_{exp} is given by

$$A_{\text{exp}} = 1 - \frac{N_{\beta\gamma}(J^-)}{N_{\beta\gamma}(J^+)} = 1 - \frac{1 + AJ^-\Lambda + b'}{1 + AJ^+\Lambda + b'}, \quad (50)$$

where $-1 \leq J^- \leq 1$ and $-1 \leq J^+ \leq 1$ are respectively the degrees of nuclear polarization for directions of the nuclear spin which are opposite or parallel to that of the emitted positron. In the case that $J^- = -J^+$, the polarization ratio may be expressed as a function of the experimental β asymmetry:

$$R = \frac{P(J^-)}{P(J^+)} = \frac{1}{1 - A_{\text{exp}}} \left[1 - \frac{2}{\frac{GA(2 - A_{\text{exp}})}{A_{\text{exp}}(1 + b')(\Omega_1 + \Omega_2)} + 1} \right]. \quad (51)$$

Considering only axial and vector couplings as applies to a pure GT transition, and ignoring the recoil order corrections discussed in Section 2.3.2, the Ω factors defined above take the following specific expressions:

$$\Omega_1^{V,A} = \frac{1}{\Lambda} \frac{\langle \epsilon(\vec{r}) \left(\frac{\gamma_z}{\gamma} (\mathcal{R}\hat{J}) \cdot \hat{n} + \left(1 - \frac{\gamma_z}{\gamma}\right) (\hat{p} \cdot \hat{J}) (\mathcal{R}\hat{p}) \cdot \hat{n} \right) \rangle}{\langle \epsilon(\vec{r}) \beta (\mathcal{R}\hat{p}) \cdot \hat{n} \rangle}, \tag{52}$$

$$\Omega_2^{V,A} = \frac{1}{\Lambda} \frac{\langle \epsilon(\vec{r}) \beta \alpha Z \frac{m}{p} (\mathcal{R}(\hat{p} \times \hat{J})) \cdot \hat{n} \rangle}{\langle \epsilon(\vec{r}) \beta (\mathcal{R}\hat{p}) \cdot \hat{n} \rangle}, \tag{53}$$

while the sensitivity to Δ of the measured polarizations ratio is given by

$$\frac{R}{R_0} = 1 - k \frac{\Delta}{1 + 4 \frac{A_{\text{exp}}(\Omega_1^{V,A} + \Omega_2^{V,A})}{(2 - A_{\text{exp}}) + A_{\text{exp}}(\Omega_1^{V,A} + \Omega_2^{V,A})} \Delta} \quad \text{with} \tag{54}$$

$$R_0 = \frac{1}{1 - A_{\text{exp}}} \left[1 - \frac{2}{\frac{(2 - A_{\text{exp}})}{A_{\text{exp}}(\Omega_1^{V,A} + \Omega_2^{V,A})} + 1} \right] \quad \text{and} \tag{55}$$

$$k = 8 \frac{A_{\text{exp}}(\Omega_1^{V,A} + \Omega_2^{V,A})(2 - A_{\text{exp}})}{(2 - A_{\text{exp}})^2 - (A_{\text{exp}}(\Omega_1^{V,A} + \Omega_2^{V,A}))^2}, \tag{56}$$

while the following approximation

$$\Omega_1^{V,A} + A\Omega_2^{V,A} \approx \Omega_1^{V,A} + \Omega_2^{V,A} \tag{57}$$

was also introduced. Note that since recoil corrections are ignored here and since $A = 1$ in the ^{12}N case, $\Omega_1^{V,A}$ and $\Omega_2^{V,A}$ are not directly observable through the experiment. Their determination requires a specific Monte Carlo calculation. The GEANT code was used to simulate positron trajectories, with routines added to compute positron spin rotation along these trajectories. In vacuum, spin rotates according to the Bargmann–Michel–Telegdi equation [62,63]. In matter, only Coulomb and Bhabha scattering were included as depolarizing processes. Depolarization by bremsstrahlung was neglected since in the present situation, the energy lost through bremsstrahlung is about 60 times less than the energy lost through multiple scattering. Spin rotation due to multiple scattering was computed from the momentum rotation given by GEANT [24]. For Coulomb and Bhabha scattering the spin rotates in the same plane as the momentum by an angle $\alpha = (1 - m/E)\eta$ where η is the momentum rotation angle [25]. The calculation for the Ω factors simulated some $\sim 6.5 \times 10^3$ positron trajectories in the experimental set-up, given initial angular and momentum distributions of positrons as produced in the decay of unpolarized ^{12}N , with the results

$$\Omega_1^{V,A} = 1.0121 \pm 0.0009, \quad \Omega_2^{V,A} = (-4.4 \pm 2.5) \times 10^{-5}, \tag{58}$$

thus leading to the following values for R_0 and k whose expressions are given in (55) and (56):

$$\begin{aligned} R_0 &= 0.99672 \pm 0.00024 \quad \text{and} \quad k = 1.0991 \pm 0.0012 \quad \text{for window-A,} \\ R_0 &= 0.99686 \pm 0.00022 \quad \text{and} \quad k = 1.0511 \pm 0.0012 \quad \text{for window-B.} \end{aligned} \tag{59}$$

These are the values quoted in (11).

The above corrections combine two different effects: a straightforward geometrical one — the finite acceptance of the spectrometer — and spin rotation.¹² When ignoring the spin rotation matrix by setting it by hand to the identity matrix in (52) and (53), these corrections may be separated, on the one hand, into a purely geometric one applied onto the polarizations ratio at positron emission, and on the other hand, a correction due to the rotation of the different spin components. Under these assumptions that $\mathcal{R} = \mathbf{I}$, $\epsilon(\vec{r}) = \text{constant}$ and $\hat{n} = \hat{z}$, the Monte Carlo evaluation of (52) and (53) gives

$$\Omega_1^{V,A}(\mathcal{R} = \mathbf{I}) = 1.0189 \pm 0.0001, \quad \Omega_2^{V,A}(\mathcal{R} = \mathbf{I}) \approx 0. \quad (60)$$

Consequently the difference between (58) and (60) is due to the rotation of the positron spin in the magnetic field.

References

- [1] Review of particle properties, Eur. Phys. J. C 15 (2000) 95–110.
- [2] P. Langacker (Ed.), Precision Tests of the Standard Electroweak Model, Advanced Series on Directions in High Energy Physics, Vol. 14, World Scientific, 1995.
- [3] P. Langacker (Ed.), Precision Tests of the Standard Electroweak Model, Advanced Series on Directions in High Energy Physics, Vol. 14, World Scientific, 1995, pp. 545–598, 657–765, 786–840.
- [4] M. Allet et al., Phys. Lett. B 383 (1996) 139.
- [5] N. Severijns et al., Phys. Rev. Lett. 70 (1993) 4047, Erratum: Phys. Rev. Lett. 73 (1994) 611.
- [6] P. Quin, T. Girard, Phys. Lett. B 29 (1989) 29.
- [7] J. Govaerts, M. Kokkoris, J. Deutsch, J. Phys. G 21 (1995) 1675.
- [8] E. Thomas, Recherche de courants droitiers par une mesure de polarisation des positrons émis par les noyaux ¹²N polarisés, PhD dissertation, Catholic University of Louvain, July 1997, unpublished.
- [9] J. Liechti et al., Nucl. Phys. A 533 (1991) 292.
- [10] E.M. Rimmer, P.S. Fisher, Nucl. Phys. A 108 (1968) 561.
- [11] F. Ajzenberg-Selove, Nucl. Phys. A 506 (1990) 100.
- [12] A. Lundby, Prog. Elem. Part. Cosmic Ray Phys. 5 (1960) 1.
- [13] L. Dick, L. Feuvrais, L. Madansky, V.L. Telegdi, Phys. Lett. 3 (1963) 326.
- [14] G. Gerber et al., Phys. Rev. D 15 (1977) 1189.
- [15] J. van House, P.W. Zitzewitz, Phys. Rev. A 29 (1984) 66.
- [16] J. Govaerts, Positronium Spectroscopy in a Magnetic Field, Internal Report UCL-IPN-93-R02, August 1993, unpublished.
- [17] R. Prieels, Tests de symétries dans les processus β -nucléaires: techniques de polarisation, in: École Internationale Joliot-Curie, Maubuisson, France, 11–16 September 1995.
- [18] R.M. Singru, K.B. Lal, At. Data Nucl. Data Tables 17 (1976) 271–409.
- [19] J.D. Jackson, S.B. Treiman, H.W. Wyld Jr., Phys. Rev. 106 (1957) 517.
- [20] J. Govaerts, Polarisation-Asymmetry Correlation in β -Decay of ¹⁰⁷In and ¹²N, Internal Report UCL-IPN-95-R04, June 1995.
- [21] J.D. Jackson, S.B. Treiman, H.W. Wyld Jr., Nucl. Phys. 4 (1957) 206.
- [22] L. Grenacs, Annu. Rev. Nucl. Part. Sci. 35 (1985) 455, and references therein.

¹² The magnetic field inhomogeneity within the positron stopping region has a negligible influence on the value for $\Omega_1^{V,A}$ which does not change if one sets in (52) $\epsilon(\vec{r})$ to a constant quantity and $\hat{n} = \hat{z}$, \hat{z} being the magnetic field symmetry axis.

- [23] B.R. Holstein, private communication, 1992.
- [24] R. Brun et al., GEANT3.16 User's Guide, CERN Program Library Office, 1993.
- [25] C. Bouchiat, J.M. Lévy-Leblond, *Nuovo Cimento* 33 (1964) 193.
- [26] F. Gimeno-Nogués, Test de la violation de la parité par une mesure de polarisation beta de noyaux ^{107}In polarisés, PhD dissertation, Catholic University of Louvain, January 1994, unpublished.
- [27] C. Dauwe, M. Tsumbu, *Phys. Rev. B* 40 (1992) 9.
- [28] W. Brandt, R. Paulin, *Phys. Rev. Lett.* 21 (1968) 193.
- [29] J. Deutsch, P.A. Quin, in: P. Langacker (Ed.), Precision Tests of the Standard Electroweak Model, Advanced Series on Directions in High Energy Physics, Vol. 14, World Scientific, 1995, pp. 786–840.
- [30] P. Herczeg, in: P. Langacker (Ed.), Precision Tests of the Standard Electroweak Model, Advanced Series on Directions in High Energy Physics, Vol. 14, World Scientific, 1995, pp. 706–766.
- [31] T.D. Lee, C.N. Yang, *Phys. Rev.* 104 (1956) 254.
- [32] C. Itzykson, J.-B. Zuber, *Quantum Field Theory*, McGraw-Hill, New York, 1980.
- [33] R.N. Mohapatra, J.C. Pati, *Phys. Rev. D* 11 (1975) 2558.
- [34] G. Senjanovic, R.N. Mohapatra, *Phys. Rev. D* 5 (1975) 1502.
- [35] G. Senjanovic, *Nucl. Phys. B* 153 (1979) 344.
- [36] A.S. Carnoy, J. Deutsch, T.A. Girard, R. Prieels, *Phys. Rev. Lett.* 65 (1990) 3249.
- [37] A.S. Carnoy, J. Deutsch, T.A. Girard, R. Prieels, *Phys. Rev. C* 43 (1991) 2825.
- [38] V.A. Wichers et al., *Phys. Rev. Lett.* 58 (1987) 1821.
- [39] Review of particle properties, *Eur. Phys. J. C* 15 (2000) 695, completed by: J. Reich et al., *Nucl. Instrum. Methods A* 440 (2000) 535.
- [40] Review of particle properties, *Eur. Phys. J. C* 15 (2000) 695.
- [41] T. Bowles, private communication.
- [42] I. Towner, The current status of V_{ud} , nucl-th/9809087.
- [43] H. Klapdor-Kleingrothaus et al., *Phys. Lett. B* 374 (1996) 7.
- [44] H. Klapdor-Kleingrothaus, *Int. J. Mod. Phys. A* 13 (1998) 3953.
- [45] P. Langacker, S. Uma Sankar, *Phys. Rev. D* 40 (1989) 1569.
- [46] A. Jodidio et al., *Phys. Rev. D* 34 (1986) 1967, Erratum: *Phys. Rev. D* 37 (1988) 237.
- [47] G. Beall et al., *Phys. Rev. Lett.* 48 (1982) 848.
- [48] G. Beall et al., *Phys. Rev. Lett.* 48 (1982) 1252.
- [49] P. Langacker, R. Mohapatra, private communication.
- [50] F. Abe et al., *Phys. Rev. Lett.* 74 (1995) 2900.
- [51] S. Abachi et al., *Phys. Rev. Lett.* 76 (1996) 3271.
- [52] J. Ng, private communication to J. Behr.
- [53] R. Mohapatra, private communication.
- [54] P. Herczeg, *Phys. Rev. D* 34 (1986) 3449.
- [55] J. Govaerts, Heavy Charged Gauge Boson Production at CDF and Left–Right Symmetric Models, Internal Report UCL-IPN-95-R05, July 1995.
- [56] Super-Kamiokande collaboration, Y. Fukuda et al., *Phys. Rev. Lett.* 81 (1998) 1562.
- [57] P. Herczeg, private communication.
- [58] J. Deutsch, in: Proc. SPIN94, Bloomington, IN, USA, September 15–22, 1994.
- [59] P. Langacker, private communication.
- [60] R. Prieels et al., experiment PSI R-97-06; P. Van Hove, PhD dissertation, Catholic University of Louvain, December 2000, unpublished.
- [61] J. Govaerts, Asymmetry-Longitudinal Polarisation Correlation in Muon Decay: a Reappraisal, Internal Report UCL-IPN-96-R02, July 1996.
- [62] V. Bargmann, L. Michel, V.L. Telegdi, *Phys. Rev. Lett.* 2 (1959) 435.
- [63] J. Govaerts, Spin 1/2 Transport in a Static Magnetic Field, Internal Report UCL-IPN95-R03, June 1995.